Effects of a laser beam profile on Zeeman electromagnetically induced transparency in the Rb buffer gas cell

2013 J. Phys. B: At. Mol. Opt. Phys. 46 075501

(http://iopscience.iop.org/0953-4075/46/7/075501)

J. Phys. B: At. Mol. Opt. Phys. **46** (2013) 075501 (10pp) doi:10.1088/0953-4075/46/7/075501

Effects of a laser beam profile on Zeeman electromagnetically induced transparency in the Rb buffer gas cell

S N Nikolić, M Radonjić, A J Krmpot, N M Lučić, B V Zlatković and B M Jelenković

Institute of Physics, University of Belgrade, Pregrevica 118, 11080 Belgrade, Serbia

E-mail: stankon@ipb.ac.rs

Received 13 September 2012, in final form 15 February 2013
Published 22 March 2013
Online at stacks.iop.org/JPhysB/46/075501

Abstract

Electromagnetically induced transparency (EIT) due to Zeeman coherences in the Rb buffer gas cell is studied for different laser beam profiles, laser beam radii and intensities from 0.1 to 10 mW cm^{-2}. EIT line shapes can be approximated by the Lorentzian for wide Gaussian laser beam (6.5 mm in diameter) if laser intensity is weak and for a Π laser beam profile of the same diameter. Line shapes of EIT become non-Lorentzian for the Gaussian laser beam if it is narrow (1.3 mm in diameter) or if it has a higher intensity. EIT amplitudes and linewidths, for both laser beam profiles of the same diameter, have very similar behaviour regarding laser intensity and Rb cell temperature. EIT amplitudes are maximal at a certain laser beam intensity and this intensity is higher for narrower laser beams. The EIT linewidth estimated at zero laser intensity is about 50 nT or 0.7 kHz, which refers to 1.5 ms relaxation times of Zeeman coherences in ^{87}Rb atoms in our buffer gas cell. Blocking of the centre of the wide Gaussian laser beam in front of the photo detector yields Lorentzian profiles with a much better contrast to the linewidth ratio for EIT at higher intensities, above ∼2 mW cm^{-2}.

(Some figures may appear in colour only in the online journal)

1. Introduction

Electromagnetically induced transparency (EIT) [1], a narrow resonance in the transmission of a laser beam through coherent media, is essential for subjects like slow and stored light [2], lasing without inversion [3], frequency mixing [4], Kerr nonlinearities [5] etc. Interest in EIT is due to the development of important devices based on EIT, such as atomic frequency standards [6] and magnetometers [7]. For such applications, the EIT linewidth is the most important resonance parameter. The narrow sub-natural Zeeman EIT resonances (EIT resonances for short) examined in this paper are attributed to the long-lived ground state Zeeman coherence. The same phenomenon was first known as the ground state Hanle effect, named by Dupont-Roc [8, 9]. The effect was later related to linear dichroism [10, 11]. In the past decade, the ground state Hanle effect has been reinterpreted in terms of EIT [12] or Zeeman EIT [13, 14]. Sub-natural EIT resonances are closely related to magneto-optical rotation (NMOR) of linearly polarized light, first studied in [15]. Similar to EIT, ultra-narrow NMOR resonances [15, 16] have found useful applications as a very sensitive technique for measuring weak magnetic fields. Recently, correlations of intensity fluctuations have been studied in NMOR experiments and reported in [17, 18]. More on magneto-optical effects, EIT and NMOR can be found in [11, 19] and references therein.

For some applications and experiments, the EIT line shape is of the highest interest, for instance in the storage of light in atomic ensembles. The product of the pulse delay and pulse broadening, which is the figure of merit in such experiments, depends not only on the steepness of the EIT resonance but also on its shape [20]. The behaviour of the EIT line shape in terms of the experimental parameters is thus of great scientific and practical importance. The EIT line shape in alkali vapours contained in gas cells is altered from the fundamental Lorentzian shape of atomic resonances by many factors. The way these factors affect the EIT depends on the type of gas cell. In vacuum cells, a thermal motion of atoms affects the shape of

the EIT through a transit time effect and Doppler broadening. While these factors prevail at a lower laser power, the power broadening determines the linewidths at laser powers near saturation levels. The behaviour of the EIT as a function of the laser beam diameter [21], optical depth [22], laser intensity [23, 24] and laser beam profile [25–28] was investigated. When alkali atoms are in a cell with buffer gas atoms, the interaction time of the alkali atoms with the laser beam is considerably increased. The linewidths, controlled here by the ground state relaxation time and the laser power, are reduced by several orders of magnitude due to the Dicke effect [29]. Linewidths as narrow as 30 Hz were obtained [30]. A non-Lorentzian line shape of the EIT, with the narrower central part of the line than in a pure Lorentzian, obtained in buffer gas cells for laser beams of small diameter, was explained by the diffusion of atoms out and then back to the laser beam. Such repeated atom–light interaction effectively enables Ramsey induced narrowing and non-Lorentzian line shape for the EIT [31, 32]. Theoretical study of a simple Λ scheme, with two ground state hyperfine levels as two lower levels, has shown that, under the assumption of immovable alkali atoms in the buffer gas, such non-Lorentzian line shape for large diameter laser beams is due to the contribution from atoms in the wings of the laser Gaussian profile [25]. Since EIT resonance contrast and linewidth depend on the cell temperature, one has to find the optimum operating temperature for achieving the maximum line contrast and the minimum linewidth. Cell temperature affects the hyperfine coherences differently to the Zeeman coherences. For the former, it is found that linewidths for the same laser intensity are narrower as the cell temperature increases. The linewidth of EIT resonances due to Zeeman coherences on the other hand, are nearly independent of the cell temperature [33].

The dependence of EIT line shapes and linewidths in buffer gas cells on the laser intensity was studied both theoretically and experimentally. Theoretical models are mainly based on a three level atomic system which allows analytic [25] and perturbative solutions [34]. Numerical modelling of an EIT in the buffer gas cell that takes into account velocity changing collisions of Rb atoms due to their thermal motion, explains the elimination of Doppler shifts and the strong Dicke-type narrowing of EIT resonances [30].

In [25], the effects of the laser intensity radial profile on the linewidth and contrast were investigated. Several experiments confirm a general trend found in the models that the linewidth for a hyperfine configuration increases linearly with the intensity, for lower laser intensities [30, 35] and nonlinearly at higher laser intensities, above the saturation limit [25]. Theoretical studies of the EIT line shapes are mainly done assuming a Π radial intensity profile of laser radiation. Experiments, on the other hand, use Gaussian or Gaussian-like laser beams profiles. The discrepancies observed between a calculated [23] and measured [24] linewidth dependence on laser intensity for hyperfine EIT might be due to the different radial laser beam intensity profiles. Few papers dealing with the issues of different laser beam profiles and EIT in buffer gas [25] and vacuum cells [26], have shown theoretically that the radial intensity profile significantly affects the EIT line shape. Most studies dealing with EIT line shapes and their dependences on the laser intensity and beam diameter, as well as on the buffer gas temperature, are for a pump–probe hyperfine configuration. There are no such studies for Zeeman EIT in a Hanle configuration.

This work investigates the behaviour of the Zeeman EIT resonances in the buffer gas cell for different laser beam radial profiles and diameters. We use the Hanle configuration in which a single, linearly polarized laser beam is resonant to the $F_g = 2 \rightarrow F_e = 1$ hyperfine transitions of the D_1 line of ^{87}Rb. The detuning of σ^+ and σ^- components of the laser beam was done by scanning the external magnetic field around zero. We obtain EIT resonances by measuring the laser transmission as a function of the applied magnetic field. The two laser beam radial profiles, Gaussian (1.3 and 6.5 mm in diameter) and Π profile (6.5 mm in diameter), were used in our study. We have also studied the EIT detected in the wings of the wide Gaussian laser beam. Thus, in this work we were able to test previously suggested effects of laser beam profiles on the EIT. According to [25, 27, 28] the line shape of the EIT is different for Gaussian and Π radial laser intensity profiles, with the former typically giving non-Lorentzian EIT resonance. Theoretical work in [25] for the three level Λ atomic scheme, shows that, when the atomic diffusion is neglected and for the same laser intensity and diameter, EIT resonances are wider and have larger amplitudes for a Π-shaped beam than for a Gaussian beam.

We develop a theoretical model based on self-consistent Maxwell–Bloch equations for the evolution of the Rb ensemble density matrix and the laser electric field in the Rb vapour. The model takes into account the collisions of Rb atoms with Ne as the buffer gas atoms through the diffusion of the Rb atoms and total depolarization of the Rb excited state. Collisional relaxation of the Rb ground state is treated using separate relaxation constants for populations and coherences. It is assumed that collisional broadening enables the approximation of the motionless atoms for longitudinal velocities. An arbitrary incident radial laser beam profile is supplied as a boundary condition for the electric field.

2. Theory and theoretical results

The starting point in calculating Zeeman EIT resonances related to the D_1 line transition $F_g = 2 \rightarrow F_e = 1$ in ^{87}Rb contained in the buffer gas cell are optical Bloch equations (OBEs) for the Rb density matrix $\hat{\rho}$.

$$\frac{\partial \hat{\rho}}{\partial t} = D\nabla^2\hat{\rho} - \frac{\mathrm{i}}{\hbar}[\hat{H}_{\mathrm{atom}}(B) + \hat{V}_{\mathrm{int}}(\mathbf{r}, t), \hat{\rho}] + \left(\frac{\partial \hat{\rho}}{\partial t}\right)_{\mathrm{SE}} + \left(\frac{\partial \hat{\rho}}{\partial t}\right)_{\mathrm{coll}}, \quad (1)$$

where

$$\hat{H}_{\mathrm{atom}}(B) = \sum_{j=-F_g}^{F_g} \hbar\omega_{F_g,j}(B)|F_g, j\rangle\langle F_g, j| + \sum_{F_e=1}^{2}\sum_{k=-F_e}^{F_e} \hbar\omega_{F_e,k}(B)|F_e, k\rangle\langle F_e, k|, \quad (2)$$

is the atomic Hamiltonian corresponding to ground (excited) states $|F_g, j\rangle \equiv |F_g, m_{g_j} = j\rangle$ ($|F_e, k\rangle \equiv |F_e, m_{e_k} = k\rangle$) with

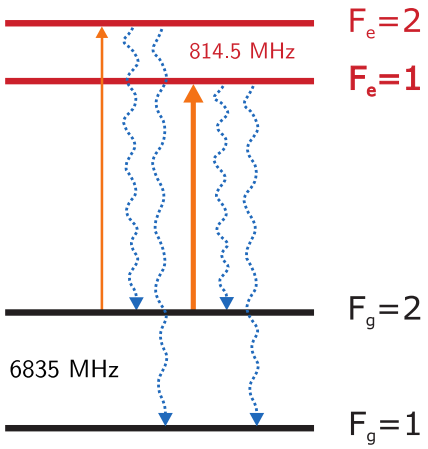

Figure 1. Energy level diagram for D_1 line transitions considered in the theoretical model. Solid lines represent transitions induced by the laser, while dotted lines correspond to possible spontaneous emission channels from excited levels. Frequency differences between adjacent hyperfine levels are shown.

Zeeman-shifted energies $\hbar\omega_{F_g,j}(B) = \hbar\omega_{F_g,0} + \mu_B g_{Fg} B m_{g_j}$ ($\hbar\omega_{F_e,k}(B) = \hbar\omega_{F_e,0} + \mu_B g_{Fe} B m_{e_k}$). μ_B is the Bohr magneton and g_{Fg} and g_{Fe} are the Landé factors for the appropriate hyperfine levels. Laser–atom interaction is given by

$$\hat{V}_{\rm int}(\mathbf{r},t) = -\sum_{j=-F_g}^{F_g}\sum_{F_e=1}^{2}\sum_{k=-F_e}^{F_e}\mathbf{E}(\mathbf{r},t) \cdot \mathbf{d}_{F_e,k}^{F_g,j}(|F_g,j\rangle\langle F_e,k| + |F_e,k\rangle\langle F_g,j|), \tag{3}$$

where $\mathbf{E}(\mathbf{r},t)$ is the laser electric field and $\mathbf{d}_{F_e,k}^{F_g,j}$ denotes the atomic electric dipole moment $\langle F_g, j|e\hat{\mathbf{r}}|F_e,k\rangle$ for the transition between states $|F_g, j\rangle$ and $|F_e,k\rangle$. The energy level diagram given in figure 1 shows hyperfine levels either coupled to the laser light or populated due to spontaneous emission. Due to the pressure-broadening of the lines in buffer gas cells, two excited levels $F_e = 1$ and $F_e = 2$ are taken to be coupled by the laser with the ground state level $F_g = 2$. Equations related to the ground state level $F_g = 1$ are not considered since that level is not coupled by the laser.

Collisions with the buffer gas have several effects. First, they lead to a diffusive motion of Rb atoms that is included through the first term on the right-hand side of (1) with D as the diffusion coefficient. Second, we assume total collisional depolarization of the excited state [36, 37] with rate Γ_d, that equalizes the populations and destroys the coherences among the Zeeman excited state sublevels within each excited state manifold $F_e = 1$ and $F_e = 2$. The collisions with the buffer gas also lead to the broadening of the optical transition described by the constant Γ_c while together with the Rb–Rb collisions lead to the relaxation of the ground states that is treated by two relaxation constants, γ_p for populations and γ_c for coherences. For the buffer gas pressure of 30 Torr the collisional broadening of approximately 300–400 MHz is comparable with the Doppler width, so that the approximation of the motionless atoms is used for the longitudinal velocities.

In the rotating wave approximation the OBEs for the density matrix elements $\rho_{F_2,m_2}^{F_1,m_1} \equiv \langle F_1, m_1|\hat{\rho}|F_2,m_2\rangle$ of a moving atom have the form

$$\frac{\partial\rho_{F_e,k}^{F_e,j}}{\partial t} = D\nabla^2\rho_{F_e,k}^{F_e,j} + (\mathrm{i}(\omega_{F_e,k} - \omega_{F_e,j}) - \Gamma)\rho_{F_e,k}^{F_e,j} - \Gamma_d\left(\rho_{F_e,k}^{F_e,j} - \frac{\pi_{F_e}\delta_{jk}}{2F_e+1}\right) + \frac{\mathrm{i}}{\hbar}\sum_{\ell=-F_g}^{F_g}\left(\tilde{\rho}_{F_g,\ell}^{F_e,j}\left(V_{F_e,k}^{F_g,\ell}\right)_+ - \left(V_{F_g,\ell}^{F_e,j}\right)_-\tilde{\rho}_{F_e,k}^{F_g,\ell}\right), \tag{4a}$$

$$\frac{\partial\tilde{\rho}_{F_g,j}^{F_e,k}}{\partial t} = D\nabla^2\rho_{F_g,j}^{F_e,k} + \left(\mathrm{i}(\omega + \omega_{F_g,j} - \omega_{F_e,k}) - \frac{\Gamma_c}{2}\right)\tilde{\rho}_{F_g,j}^{F_e,k} + \frac{\mathrm{i}}{\hbar}\left(\sum_{F_e=1}^{2}\sum_{m=-F_e}^{F_e}\rho_{F_e,m}^{F_e,k}\left(V_{F_g,j}^{F_e,m}\right)_- - \sum_{\ell=-F_g}^{F_g}\left(V_{F_g,\ell}^{F_e,k}\right)_-\rho_{F_g,j}^{F_g,\ell}\right), \tag{4b}$$

$$\frac{\partial\rho_{F_g,k}^{F_g,j}}{\partial t} = D\nabla^2\rho_{F_g,k}^{F_g,j} + \mathrm{i}\left(\omega_{F_g,k} - \omega_{F_g,j}\right)\rho_{F_g,k}^{F_g,j} - \gamma_p\delta_{jk}\left(\rho_{F_g,k}^{F_g,j} - \frac{1-\pi_e}{n_g}\right) - \gamma_c(1-\delta_{jk})\rho_{F_g,k}^{F_g,j} + \frac{\mathrm{i}}{\hbar}\sum_{F_e=1}^{2}\sum_{m=-F_e}^{F_e}\left(\tilde{\rho}_{F_e,m}^{F_g,j}\left(V_{F_g,k}^{F_e,m}\right)_- - \left(V_{F_e,m}^{F_g,j}\right)_+\tilde{\rho}_{F_g,k}^{F_e,m}\right) + (-1)^{j+k}\sum_{F_e=1}^{2}(2F_e+1)\Gamma_{F_e\to F_g}\sum_{q=-1}^{1}\rho_{F_e,k+q}^{F_e,j+q}\mathcal{C}_q(F_e,F_g;j,k), \tag{4c}$$

where $\mathcal{C}_q(F_e,F_g;j,k) = \begin{pmatrix} F_e & 1 & F_g \\ j+q & -q & -j\end{pmatrix}\begin{pmatrix} F_e & 1 & F_g \\ k+q & -q & -k\end{pmatrix}$.

Diagonal density matrix elements $\rho_{F_g,j}^{F_g,j}$ ($\rho_{F_e,k}^{F_e,k}$) are populations of $|F_g, j\rangle$ ($|F_e,k\rangle$) Zeeman sublevels, while off-diagonal elements $\rho_{F_g,k}^{F_g,j}$ ($\rho_{F_e,k}^{F_e,j}$) are appropriate Zeeman coherences between ground (excited) Zeeman sublevels. Fast oscillations of the optical coherences $\rho_{F_g,k}^{F_e,j}$ were eliminated by standard substitution $\rho_{F_g,k}^{F_e,j} = \tilde{\rho}_{F_g,k}^{F_e,j}\exp(-\mathrm{i}\omega t)$, where ω is the laser frequency in the laboratory frame. $\Gamma_{F_e\to F_g}$ is the decay rate from F_e to one F_g ground hyperfine level given by

$$\Gamma_{F_e\to F_g} = (2J_e+1)(2F_g+1)\begin{Bmatrix} J_g & J_e & 1 \\ F_e & F_g & I\end{Bmatrix}^2\Gamma, \tag{5}$$

where J represents the electron angular momentum quantum numbers and $I = 3/2$ is the nuclear angular momentum of ^{87}Rb. π_{F_e} is the population of the excited level F_e, $\pi_e = \sum_{F_e=1}^{2}\pi_{F_e}$ is the total population of exited levels $F_e = 1$ and $F_e = 2$ and $n_g = 2(2I+1)$ is the total number of substates in the ground state levels $F_g = 1$ and $F_g = 2$. Coherences among excited states belonging to different manifolds are neglected.

In a general case, the laser electric field is given by

$$\mathbf{E}(\mathbf{r},t) = \mathbf{e}_x E_{0x}(\mathbf{r},t)\cos(\omega t - \mathbf{kr}) + \mathbf{e}_y E_{0y}(\mathbf{r},t)\cos(\omega t - \mathbf{kr} + \varphi). \tag{6}$$

For symmetry reasons it is better to express the laser electric field in terms of the spherical basis unit vectors $\mathbf{u}_{\pm1} = (\mp\mathbf{e}_x - \mathrm{i}\mathbf{e}_y)/\sqrt{2}$

$$\mathbf{E} = (\mathbf{u}_{+1}E_{+1,+} + \mathbf{u}_{-1}E_{-1,+})\,\mathrm{e}^{\mathrm{i}(\omega t - \mathbf{kr})} + (\mathbf{u}_{+1}E_{+1,-} + \mathbf{u}_{-1}E_{-1,-})\,\mathrm{e}^{-\mathrm{i}(\omega t - \mathbf{kr})}, \tag{7}$$

where we used the notation $E_{\pm1,\pm} = (\mp E_{0x} + \mathrm{i}\mathrm{e}^{\pm\mathrm{i}\varphi}E_{0y})/(2\sqrt{2})$. Terms $\left(V_{F_e,k}^{F_g,j}\right)_{\pm}$ in OBEs (4) are of the form

$$\left(V_{F_e,k}^{F_g,j}\right)_{\pm} = -\left(d_{F_e,k}^{F_g,j}\right)_{-1} E_{-1,\pm} - \left(d_{F_e,k}^{F_g,j}\right)_{+1} E_{+1,\pm}. \quad (8)$$

Here $(d_{F_e,k}^{F_g,j})_q$ is the spherical component of the electric dipole matrix element that can be calculated as

$$\begin{aligned}\left(d_{F_e,k}^{F_g,j}\right)_q &= \left\langle F_g, j|\mathbf{u}_q \cdot e\hat{\mathbf{r}}|F_e, k\right\rangle \\ &= \left\langle J_g||e\hat{\mathbf{r}}||J_e\right\rangle (-1)^{J_g+I+j}\sqrt{(2F_g+1)(2F_e+1)(2J_g+1)} \\ &\quad \times \begin{Bmatrix} J_g & J_e & 1 \\ F_e & F_g & I \end{Bmatrix} \begin{pmatrix} F_e & 1 & F_g \\ k & q & -j \end{pmatrix}, \end{aligned} \quad (9)$$

where $\left\langle J_g||e\hat{\mathbf{r}}||J_e\right\rangle$ is the reduced matrix element of the electric dipole operator between appropriate ground and excited states. Due to the relation $(d_{F_g,j}^{F_e,k})_q^* = (-1)^q (d_{F_e,k}^{F_g,j})_{-q}$, the terms $(V_{F_g,j}^{F_e,k})_{\pm}$ are completely determined by the terms $\left(V_{F_e,k}^{F_g,j}\right)_{\mp}$.

Optical Bloch equations (4) represent a set of coupled time-dependent three-dimensional partial differential equations. We are interested in the cylindrical symmetric steady state case because the coupling laser field possesses such properties. In the magnetic field B the atomic ensemble density matrix is a function of only the radial and axial space coordinates, i.e. $\hat{\rho}(\mathbf{r}, B) \to \hat{\rho}(r, z; B)$. Also, the diffusion terms have only radial and axial derivatives, i.e. $\nabla^2 \to \nabla^2(r, z)$. For a given electric field inside the cell, OBEs can be solved with boundary conditions

$$\rho_{F_g,k}^{F_g,j}(R, z; B) = \rho_{F_g,k}^{F_g,j}(r, 0; B) = \rho_{F_g,k}^{F_g,j}(r, L; B) = \frac{\delta_{jk}}{n_g}, \quad (10)$$

with all other relevant matrix elements being set to zero. R and L are the cell radius and length, respectively.

The effects of the laser propagation along the cell and induced atomic polarization of the Rb vapour are included in the following manner. When the Rb vapour ensemble density matrix $\hat{\rho}(r, z; B)$ is known, the polarization of Rb vapour having the temperature dependent density $n(T)$ is obtained as

$$\begin{aligned}\mathbf{P}(r, z; B) &= n(T)\,\mathrm{Tr}(\hat{\rho}(r, z; B)\, e\hat{\mathbf{r}}) = n(T)\,\mathrm{e}^{-\mathrm{i}(\omega t - \mathbf{kr})} \\ &\quad \times \sum_{j=-F_g}^{F_g} \sum_{F_e=1}^{2} \sum_{k=-F_e}^{F_e} \mathbf{d}_{F_e,k}^{F_g,j}\, \tilde{\rho}_{F_g,j}^{F_e,k}(r, z; B) + \text{c.c.}, \end{aligned} \quad (11)$$

where $\mathbf{d}_{F_e,k}^{F_g,j} = \mathbf{e}_x\left(\left(d_{F_e,k}^{F_g,j}\right)_{-1} - \left(d_{F_e,k}^{F_g,j}\right)_{+1}\right)/\sqrt{2} + \mathrm{i}\mathbf{e}_y\left(\left(d_{F_e,k}^{F_g,j}\right)_{-1} + \left(d_{F_e,k}^{F_g,j}\right)_{+1}\right)/\sqrt{2}$. Let $\mathcal{E}(\mathbf{r}, t; B)$ and $\mathcal{P}(\mathbf{r}, t; B)$ denote complex slowly varying envelopes of the electric field and the polarization, respectively, defined by

$$\mathbf{E}(\mathbf{r}, t; B) = \mathrm{Re}(\mathcal{E}(\mathbf{r}, t; B)\,\mathrm{e}^{-\mathrm{i}(\omega t - \mathbf{kr})}), \quad (12a)$$

$$\mathbf{P}(\mathbf{r}, t; B) = \mathrm{Re}(\mathcal{P}(\mathbf{r}, t; B)\,\mathrm{e}^{-\mathrm{i}(\omega t - \mathbf{kr})}). \quad (12b)$$

In a steady state slowly varying envelopes are related by the propagation equation

$$\frac{\partial \mathcal{E}(r, z; B)}{\partial z} = \frac{\mathrm{i}\omega}{2\epsilon_0 c}\mathcal{P}(r, z; B), \quad (13)$$

where ϵ_0 is the vacuum dielectric constant. The laser electric field at the entrance to the Rb cell (at $z = 0$) can be an arbitrary function of the radial coordinate and it is supplied as a boundary condition. The transmitted electric field (at $z = L$) is calculated using the relations (11)–(13).

In order to obtain EIT resonances from the transmitted electric field one has to solve for the ensemble density matrix and electric field in a self-consistent way for a given magnetic field B:

(i) assume that the electric field along the cell is equal to the incident laser electric field, i.e. $\mathcal{E}(r, z; B) = \mathcal{E}_{\mathrm{in}}(r)$;
(ii) calculate the elements of the ensemble density matrix $\hat{\rho}(r, z; B)$ using steady state OBEs (4) and boundary conditions (10);
(iii) calculate the electric field inside the cell $\mathcal{E}(r, z; B)$ using (11)–(13) with $\mathcal{E}(r, 0; B) = \mathcal{E}_{\mathrm{in}}(r)$ as a boundary condition;
(iv) repeat the procedure from step (ii) until self-consistency is reached.

Numerical calculations are performed using the *DOLFIN* finite element library [38] (part of *FEniCS* project [39]) and *CBC.PDESys* package [40]. Note that the EIT resonances presented in this study are obtained after normalizing calculated or measured EIT curves to the transmission at a sufficiently large magnetic field.

In order to determine the temperature dependence of EIT resonance amplitudes, calculations are performed at temperatures of 60, 75 and 82 °C. The calculated EIT resonances for a Gaussian laser beam with $1/e^2$ diameters $d = 6.5$ mm and $d = 1.3$ mm are shown in figures 2(a) and (b). It can be seen that in this temperature range stronger resonances are obtained at higher temperatures for both beam diameters due to the increased density of Rb vapour.

In figure 3 the EIT resonances for two laser beam diameters are presented together with their Lorentzian fits. While the line shapes of the EIT curves for wider laser beams are close to Lorentzian, EIT resonances with narrower laser beams show additional narrowing in the vicinity of a zero magnetic field and certainly are non-Lorentzian. These results, both for wide and narrow Gaussian laser beams, are in agreement with [25, 31].

The EIT amplitudes and linewidths shown in figure 4 are extracted from these curves for a wide Gaussian laser beam at 82 °C and laser intensity interval 0.1–10 mW cm^{-2}. The amplitude dependence on the intensity has a maximum at $I \sim 1.1$ mW cm^{-2}. Further decrease of the amplitudes is due to the increased effect of optical pumping to the non-coupled ground state level $F_g = 1$.

3. Experiment and experimental results

Zeeman EIT experiment in the Hanle configuration needs a single laser whose frequency and polarization of radiation are stable and well controlled. Essential for Zeeman EIT measurements is also the elimination of stray magnetic fields, as well as the creation of a homogeneous magnetic field over the entire Rb cell, directed along its axis. In our experiment an additional requirement is a careful control of the laser beam diameter and radial distribution of laser radiation. The schematic of the experiment is given in figure 5.

We use the external cavity diode laser whose frequency is locked to the $F_g = 2 \to F_e = 1$ transition in ^{87}Rb with the Doppler-free dichroic atomic vapour laser lock technique [41, 42]. The Gaussian laser beam profile, whose diameter is adjusted by the periscope, is obtained by the single mode optical fibre. For achieving a Π radial intensity distribution of the laser beam we use the laser beam shaper which consists of

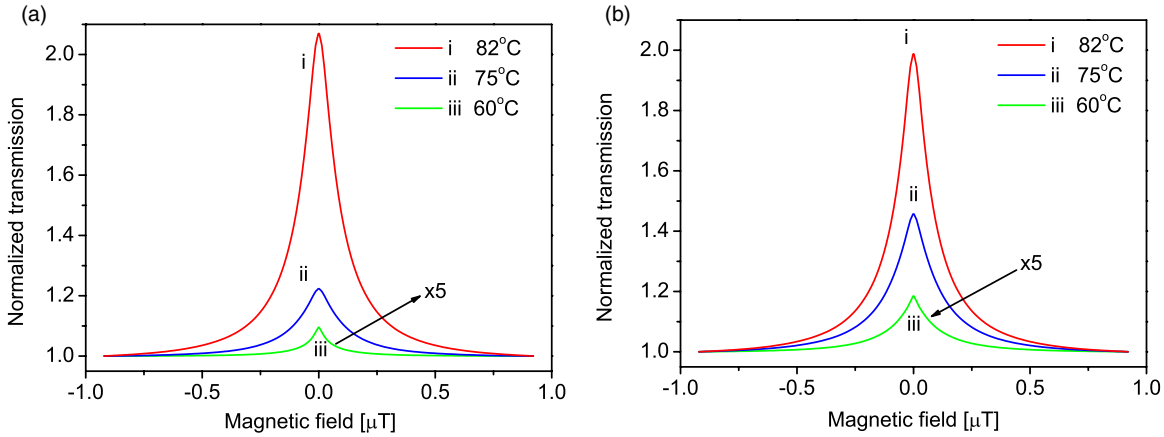

Figure 2. Theoretically obtained EIT resonances for a Gaussian laser beam of diameter (a) $d = 6.5$ mm and (b) $d = 1.3$ mm. Resonances are calculated at three temperatures: 60, 75 and 82 °C. Laser beam intensity is 1.1 mW cm^{-2}.

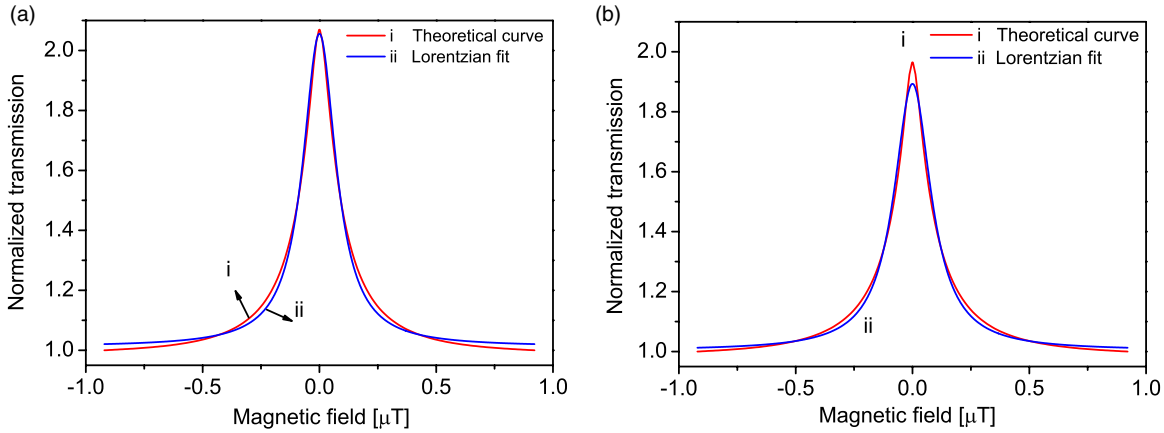

Figure 3. Theoretically obtained EIT resonances (i) and corresponding Lorentzian fits (ii) for a Gaussian laser beam of diameter (a) $d = 6.5$ mm (Adj. $R^2 = 0.997\,54$) and (b) $d = 1.3$ mm (Adj. $R^2 = 0.994\,67$). Resonances are calculated at the cell temperature of 82 °C. Laser beam intensity is 1.1 mW cm^{-2}.

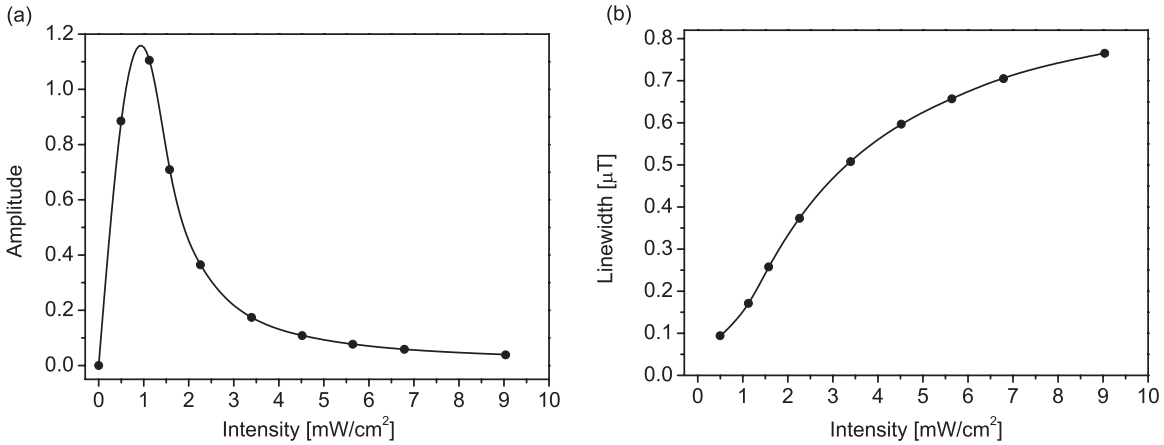

Figure 4. Calculated dependences of the EIT (a) amplitude and (b) linewidth on laser intensity for a Gaussian laser beam with a diameter of 6.5 mm at the cell temperature of 82 °C.

the beam expander, the collimator and thin foil with a 6.5 mm hole as the iris, placed over the central part of the laser beam previously expanded to approximately 20 mm in diameter. We use linearly polarized laser radiation. Linearity and orientation of the polarization is assured by the high quality polarizer and $\lambda/2$ retardation plate. Laser beam intensity is controlled by the variable neutral density filter. The Rb glass cell, 8 cm long and 25 mm in diameter with 30 Torr of Ne buffer gas, is placed in a plastic box and heated to a certain temperature by hot air circulating around the cell. The advantage of this system in comparison with electrical heating is in elimination of the stray magnetic fields introduced by the heating current

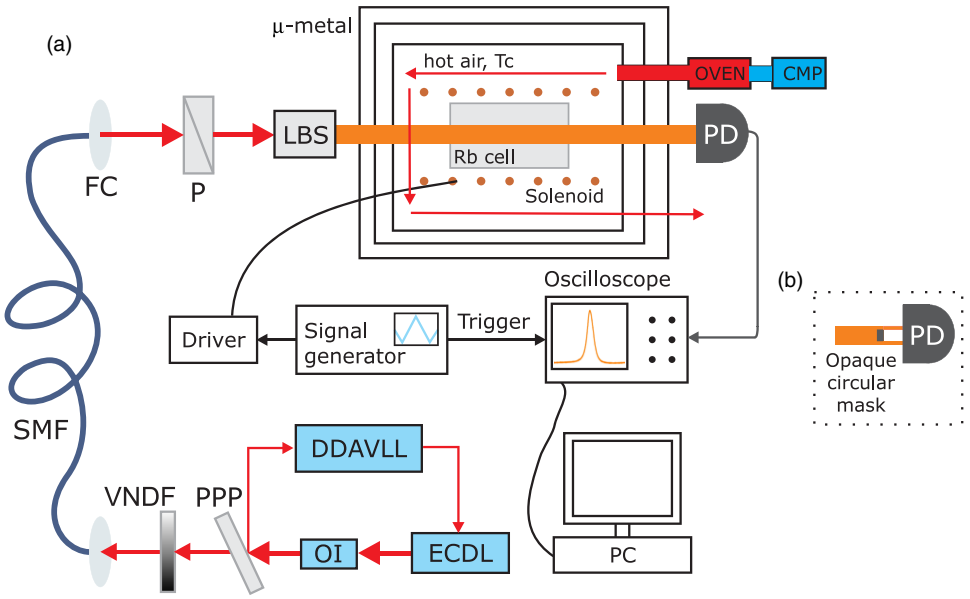

Figure 5. Experimental setup: ECDL—external cavity diode laser; OI—optical insulator; DDAVLL—Doppler-free dichroic atomic vapour laser lock; PPP—plan parallel plate; VNDF—variable neutral density filter; SMF—single-mode fibre; FC—fibre coupler; P—polarizer; LBS—laser beam shaper; PD—large area photodiode; CMP—compressor. A laser beam shaper is used to shape the diameter and the radial intensity profile of the laser beam. Detection of the whole laser beam is shown in (a). The inset in (b) presents the blockage of the laser beam centre and detection of only the outer parts of the beam.

inside μ-metal shielding. The Rb cell is shielded from external magnetic fields by the triple layer of μ-metal which reduces stray magnetic fields below 10 nT. The long solenoid around the Rb cell produces a controllable longitudinal magnetic field for the experiment in the range of $\pm$ 20 μT. The intensity of the transmitted laser light as a function of the applied magnetic field was monitored by the photodiode and recorded by the storage oscilloscope. For measuring EIT generated only by photons from the wings of the 6.5 mm Gaussian laser beam, we put an opaque round mask of 6.0 mm in diameter, after the gas cells e.g. in front of the detector.

We present our results of the EIT line shapes, amplitudes and linewidths for various cell temperatures, laser light intensities, laser beam diameters and intensity radial profiles. We use Gaussian beams of 6.5 and 1.3 mm in $1/e^2$ diameter. We also compare these resonances with corresponding ones for a Π laser beam profile of 6.5 mm in diameter. Measurements were done in the temperature range from 50 to 82 °C and for the laser intensities 0.1–10 mW cm^{-2} for a wide Gaussian beam, 0–35 mW cm^{-2} for a narrow Gaussian beam and 0–3.5 mW cm^{-2} for a Π laser beam. It was impossible to achieve a Π laser beam profile of 1.3 mm in diameter due to the pronounced diffraction on the beam shaper aperture.

Non-Lorentzian line shapes in buffer gas cells obtained with a narrow laser beam with a diameter of the order of $\lesssim$2 mm, were explained by diffusion induced Ramsey narrowing, due to coherently prepared atoms coming back to the laser beam after spending time in the dark [31, 32]. On the other hand, non-Lorentzian line shapes for the wide Gaussian laser beam are due to the contribution from the atoms in the wings of the beam [25]. It was demonstrated that in vacuum gas cells, repeated interactions of atoms, coherently prepared in the central parts of the beam, with the laser light in the wings of a wide Gaussian laser beam, leads to EIT narrowing [43]. We investigated the contribution of the outer parts of the laser beam to the overall EIT formation in the buffer gas cell, by measuring the EIT resonances after blocking the central part of the well collimated laser beam just in front of the detector.

The EIT line shapes for the wide and the narrow Gaussian laser beam, are presented in figure 6, parts (a) and (b), respectively. The EIT resonances for a 6.5 mm diameter laser beam are given for two laser intensities. At a laser intensity of 1.6 mW cm^{-2} the EIT line shape (curve (i)) fits well with the Lorentzian fit (curve (ii)). Such behaviour is found for laser intensities below $\sim$5 mW cm^{-2}. However, as the laser intensity increases, the EIT line shapes are gradually different from the Lorentzian. These results are in agreement with the EIT profiles for a Gaussian laser beam [27]. The EIT resonance measured at 9.2 mW cm^{-2} is different from its Lorentzian fit, as seen from the experimental curve (iii) and its fit (iv) in figure 6(a), respectively. The non-Lorentzian EIT line shape for the wide laser beam with a Gaussian intensity profile and higher intensity could be explained in terms of unequal light intensities within different parts of the Gaussian laser beam profile [25, 27, 28]. As suggested in [25], the sharper central peak of the EIT resonance is due to the contribution of atoms illuminated by a low intensity light in the wings of the laser beam. When the overall laser intensity is higher there is enough power at the wings of the beam to enhance this effect. Conversely, when the laser intensity is small the contribution from these segments is negligible. Thus, for lower laser intensities and wide Gaussian beams, the resonance line shapes fit very well with the Lorentzian.

Resonances obtained for the narrow Gaussian laser beam of 1.3 mm in diameter, presented in figure 6(b), have non-Lorentzian line shapes and sharp central peaks regardless of

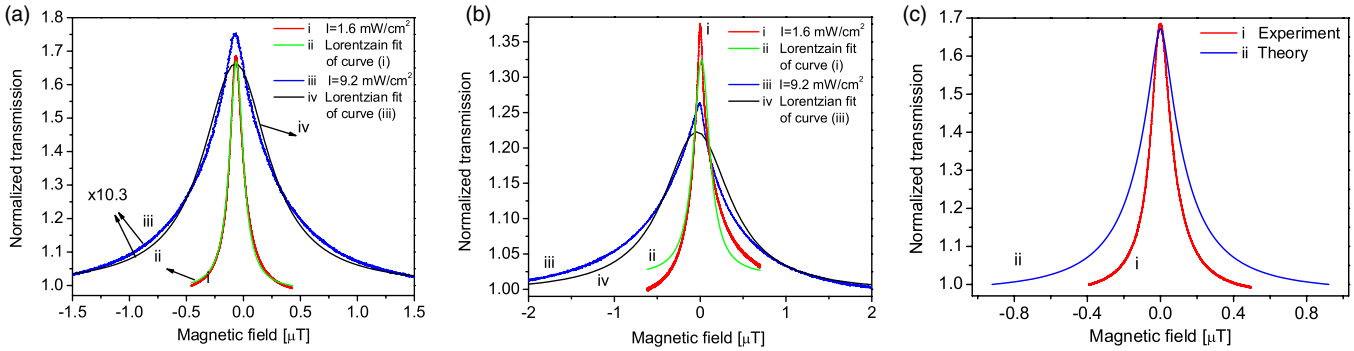

Figure 6. Measured EIT resonances for the Gaussian laser beam of diameter (a) $d = 6.5$ mm and (b) $d = 1.3$ mm. Curves (i) and (ii) are a measured EIT resonance at 1.6 mW cm^{-2} and its Lorentzian fit, respectively, while curves (iii) and (iv) correspond to the measured EIT resonance at 9.2 mW cm^{-2} and its Lorentzian fit, respectively. Note that the curves (iii) and (iv) in (a) are multiplied by 10.3 in order to present them on the same scale as curves (i) and (ii). A comparison between the measured and calculated EIT resonances (curves (i) and (ii), respectively) for a Gaussian laser beam of $d = 6.5$ mm in diameter and 1.6 mW cm^{-2} of the overall intensity is shown in (c). The cell temperature is 82 °C.

the laser intensity. The narrowing at very small magnetic fields is caused by the Ramsey effect, i.e. the diffusion of atoms out from the laser beam and then back to the interaction region as presented in [31, 32]. Non-Lorentzian line shapes for the narrow laser beam that we observed for all laser intensities, are in agreement with the diffusion induced Ramsey narrowing mechanism. Curves (ii) and (iv) in figure 6(b) are Lorentzian fits of the experimental resonances (i) and (iii) respectively, which have wider central peaks that are different from the experimental resonances. A comparison between experimentally and theoretically obtained EIT resonances for the laser beam of 6.5 mm in diameter is shown in figure 6(c). The amplitudes and line shapes of both curves (i) and (ii) are almost the same, however the linewidth of the experimental resonance is slightly narrower than its theoretical counterpart.

Resonances obtained with a Π laser beam profile of 6.5 mm in diameter have a Lorentzian line shape for all laser intensities with a similar linewidth and amplitude dependence on the laser beam intensity as for the Gaussian laser beam of the same diameter.

For the narrow Gaussian laser beam, the line shape is non-Lorentzian with a sharp central peak for all laser intensities due to diffusion induced Ramsey narrowing [31, 32]. In this case, the influence of the non-uniform beam intensity profile is marginal. A definite argument for such a conclusion could be given by a comparison with the corresponding results for the narrow Π laser beam. Unfortunately, we were not able to produce the narrow Π laser beam profile. However, indirect proof is present in [32], because there is an excellent agreement between the theory based on the narrow Π laser beam profile and the experiment with the narrow Gaussian laser beam. On the other hand, the line shape obtained with the wide Gaussian laser beam is Lorentzian for lower laser intensities. As the light intensity increases, EIT resonance line shape for the wide Gaussian laser beam becomes non-Lorentzian. Therefore, one can draw the conclusion that the diffusion induced Ramsey effect has no significant influence on the line shape for the wide Gaussian laser beam [31, 32]. Hence, non-Lorentzian line shapes at higher intensities for the wide Gaussian laser beam are due to the non-uniform laser beam profile, in line with [25, 27, 28]. This is further supported by the fact that EIT line shapes for the wide Π profile are Lorentzian for all intensities.

The line shapes of the EIT resonances measured at the cell temperatures of 50, 60 and 75 °C are qualitatively similar to theoretical ones and those shown in figure 6. However, the EIT amplitude and linewidth dependences on laser intensity are in general different at various temperatures. Figure 7 shows the EIT amplitudes and linewidths as functions of the laser beam intensity for a wide Gaussian laser beam at four temperatures. There is a strong increase in the EIT contrast associated with a higher cell temperature, as shown in figure 7(a), with the maximum obtainable temperature of the cell achieved by hot air heating of ∼82 °C. The density of Rb atoms increases rapidly with the higher temperature, reaching $\sim 5 \times 10^{11}$ cm^{-3} at 82 °C, giving stronger resonances as more atoms can undergo transition into the dark state. At even higher temperatures, radiation trapping and dark state decoherence due to Rb–Rb collisions lead to a lowering of the EIT resonances amplitudes [44, 45].

An increase of the cell temperature results in a higher optical depth, requiring a stronger light field to efficiently prepare atoms in the dark state and to obtain the peak of the laser transmission. At even larger intensities, the amplitude of the EIT resonance decreases since optical pumping into the $F_g = 1$ hyperfine state prevails coherent excitation. Indeed, when the re-pump laser is used to bring back the population to the $F_g = 2$ level, the contrast of the amplitudes increases considerably [46]. Previous analysis implies that the dependence of the EIT amplitudes on the laser intensity must possess a maximum, as shown in figure 7(a). Maximal EIT amplitude for the wide Gaussian laser beam at 82 °C is obtained for the intensity of 1.1 mW cm^{-2} which is similar to results of the theoretical model shown in figure 4(b).

While the dependence of the EIT amplitudes on the laser intensity considerably varies with the cell temperatures, the EIT linewidths have a similar dependence on the laser intensity for the whole range of cell temperatures, as shown in figure 7(b). At lower laser intensities the EIT linewidths are

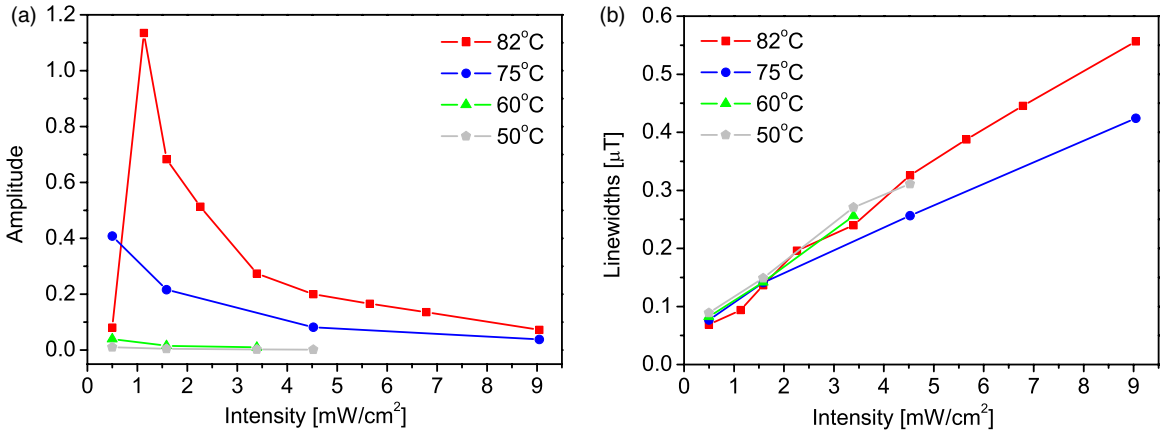

Figure 7. Experimental dependences of EIT (a) amplitudes and (b) linewidths on the overall laser intensity for a Gaussian laser beam with a diameter of 6.5 mm at four different temperatures.

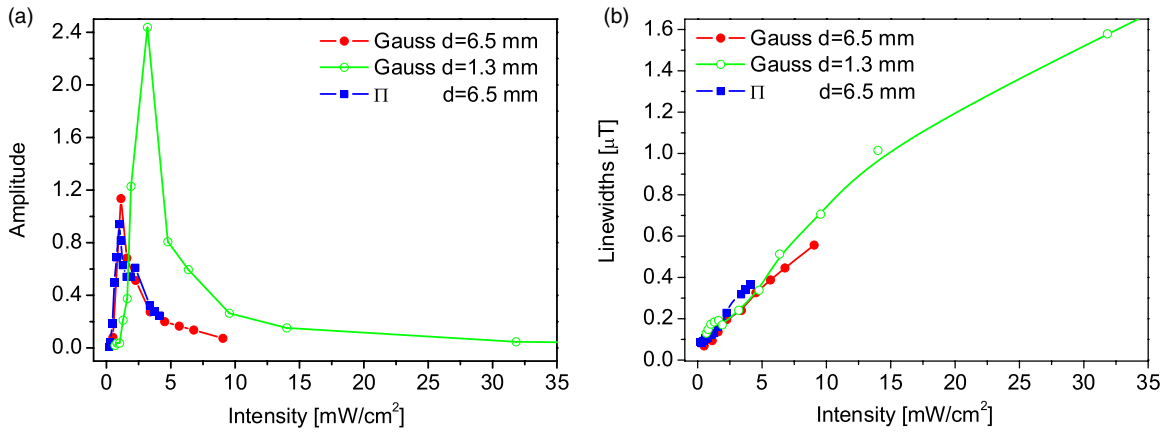

Figure 8. Experimental dependences of EIT (a) amplitudes and (b) linewidths on laser beam intensity for different laser radial profiles and diameter d: (i) Gaussian $d = 6.5$ mm, (ii) Π $d = 6.5$ mm and (iii) Gaussian $d = 1.3$ mm. Cell temperature is 82 °C.

independent of the cell temperature. Calculated linewidths, as a function of the laser intensity for 82 °C presented in figure 4(b), have a similar qualitative dependence as measured. These results are in agreement with [33] where a similar (non)dependence of Zeeman EIT on the cell temperature is obtained for cells with 1 and 10 Torr of Ne buffer gas. The estimated linewidth at zero laser intensity for a 6.5 mm laser beam diameter is about 50 nT or 0.7 kHz. This linewidth is an order of magnitude lower than in [33]. This reduction in linewidth could be due to the different buffer gas cells, but could also be attributed to the negligible stray magnetic fields inside the magnetic shielding achieved with hot air heating of the Rb cell.

The following results of the EIT line shapes, amplitudes and linewidths for different laser beams' radial profiles were obtained with a cell temperature of 82 °C. In figure 8 we show how the diameter of the Gaussian laser beam affects EIT amplitudes and linewidths. Amplitudes are much higher for the 1.3 mm than for the 6.5 mm beam diameter, as noted in figure 8(a). For the narrower laser beam, more non-coherent atoms can enter the laser beam and reach the intense central part. Thus, a lower off-resonant absorption is obtained for narrower than for wider Gaussian laser beams. Since we normalize the EIT resonance to the off-resonant transmission, a stronger peak amplitude was measured for the Gaussian beam of 1.3 mm in diameter. On the other hand, EIT linewidths for both beam diameters are nearly the same (where the laser intensity ranges overlap), as given in figure 8(b). Although a narrower laser beam gives EIT line shapes with a very narrow central peak, this has an insignificant effect on EIT linewidths.

Figure 8 also presents the dependence of EIT amplitudes and linewidths on the laser intensity for a Π laser beam profile 6.5 mm in diameter. The theoretical comparisons given in [25] show that, as the laser intensity increases, resonances for the Gaussian beam get narrower and of a slightly higher amplitude than for the Π profile. Our results in figure 8 show that in the overlapping range of laser intensities there are no significant differences in EIT amplitudes for Gaussian and a Π profile of the same diameter. EIT linewidths, almost the same at a lower laser intensity, get slightly narrower for the Gaussian beam than for the Π laser beam profile. Very small differences of EIT properties obtained with the Gaussian and Π laser beam are in contrast with the strong effects of radial intensity distribution on EIT in a vacuum gas cell [47].

In order to observe EIT developed by weak laser light in the wings of the wide Gaussian laser beam, we measured transmission of the 6.5 mm Gaussian laser beam with the central part of the beam blocked by a mask 6.0 mm in

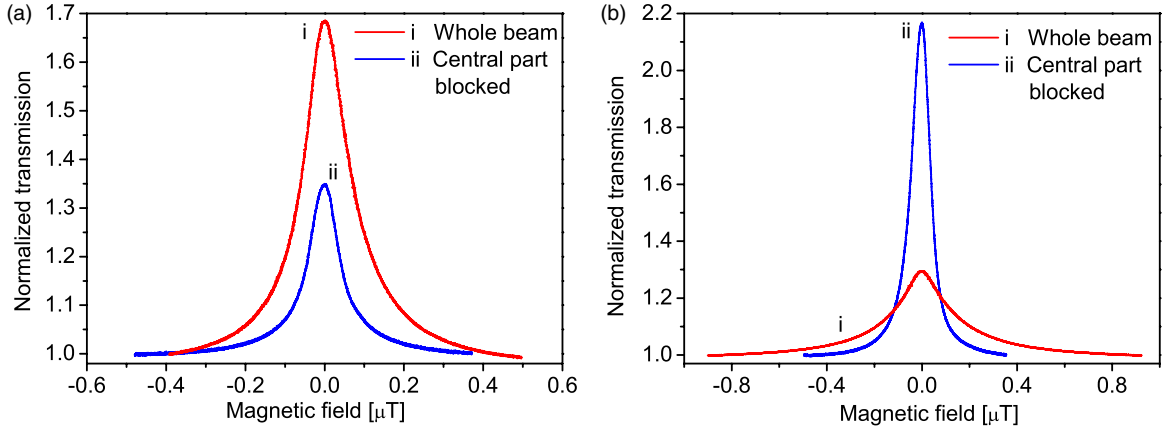

Figure 9. Measured EIT resonances for a Gaussian laser beam 6.5 mm in diameter. Marks (i) and (ii) indicate curves obtained detecting the whole beam and its outer parts only, respectively. Overall laser beam intensity is (a) 1.6 mW cm^{-2} and (b) 3.3 mW cm^{-2}.

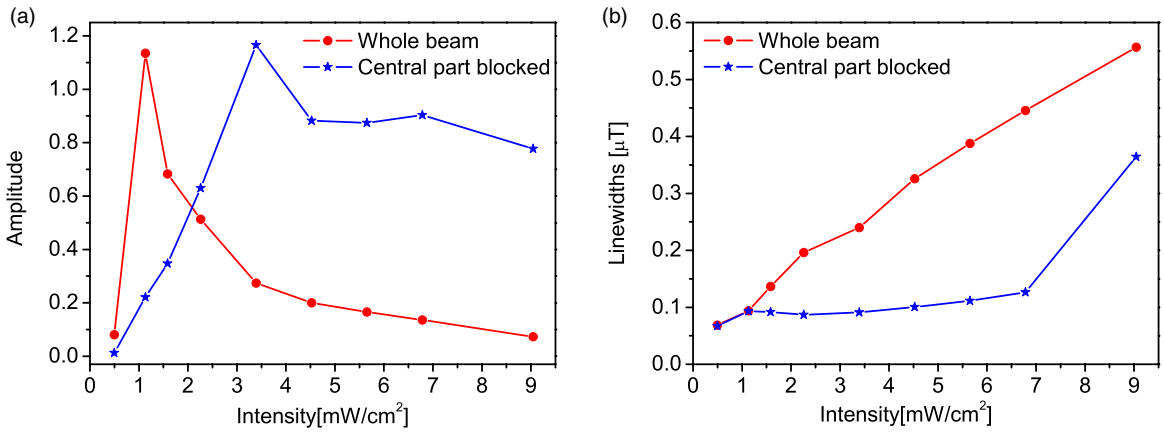

Figure 10. Experimental dependences of EIT (a) amplitudes and (b) linewidths on laser beam intensity obtained by measuring (i) the whole beam and (ii) only its outer parts. Cell temperature is 82 °C.

diameter, placed in front of the photo detector. Examples of such measurements, for two laser intensities, 1.1 and 3.3 mW cm^{-2}, are shown in figures 9(a) and (b), respectively.

EIT resonances measured by detecting the whole laser beam at lower laser intensities, have a Lorentzian line shape, in agreement with [32]. By blocking the central part of the beam, measured EIT resonances are due to the interaction of rather weak laser light in the wings of the beam with the atoms coherently prepared in the central parts of the laser beam. As we see from figure 9, the EIT resonances for the whole laser beam and for the beam whose central region is blocked, are both Lorentzian. That suggests that the diffusion-induced Ramsey effect is suppressed in this setup, likely because the atoms move mainly within the low intensity wings of the laser beam. However, we obtained interesting differences of EIT amplitudes and linewidths at different laser intensities. For the lower laser intensity, EIT resonances obtained by detecting the whole beam have a larger amplitude (figure 9(a)). As we increase the light intensity (above ∼2 mW cm^{-2}) measured resonances with the central part of the beam blocked, become more contrasted and narrower (figure 9(b)). The effect of this blocking is further investigated in figure 10 where we present dependences of EIT amplitudes and linewidths on the total intensity for these two experimental realizations.

From figure 10 we see benefits of blocking the central part of the laser beam at higher laser intensity: EIT contrast is higher and linewidths are narrower. The increase of the amplitudes is a consequence of the decreased optical pumping to the non-coupled ground state level $F_g = 1$ in the low intensity beam wings. This is in accordance with figures 4(a) and 7(a). EIT narrowing is also attributed to lower power broadening. No conclusion about the influence of Ramsey narrowing on the linewidths in figure 10 can be made due to the absence of the specific sharp central peak in the representative EIT resonances of figure 9.

4. Conclusion

We have presented experimental and theoretical results of the behaviour of Zeeman EIT resonances in a Rb buffer gas cell for different laser beam profiles, diameters and intensities. For the narrow Gaussian laser beam (1.3 mm in diameter) non-Lorentzian line shapes of EIT are obtained. The characteristic, very narrow central part of these resonances is a contribution of diffusion-induced Ramsey narrowing. We confirmed theoretical predictions that EIT resonances obtained with the wider Gaussian laser beam (6.5 mm in diameter) have different profiles at different laser intensities, a

Lorentzian-like profile for lower laser intensities and a non-Lorentzian shape with a narrower central part for higher laser intensities. In contrast to the case of the narrow laser beam, the non-Lorentzian line shape for a wider beam at higher intensities is due to the contribution of atoms from the beam's wings where the laser field is considerably lower than at the beam's centre. At lower laser beam intensities, the contribution of these segments is negligible, thus Lorentzian line shapes are obtained. Π-shaped laser beam, 6.5 mm in diameter, gives a pure Lorentzian EIT line shape.

EIT linewidths obtained either by the narrow or the wide Gaussian laser beam, for all laser intensities, are independent of the Rb temperature. The EIT with a Gaussian laser beam have the same amplitudes and are slightly narrower than those with the Π profile. About a six-fold increase in EIT contrast for higher laser intensities with a considerable decrease in linewidth was obtained simply by blocking the central part of the wide Gaussian laser beam, just in front of the photo detector. Such effects are attributed to the decreased optical pumping to the non-coupled ground state level $F_g = 1$ and reduced power broadening in the low intensity beam wings. A possible influence of the diffusion-induced Ramsey effect could not be confirmed because of the absence of a narrow peak in the EIT line shapes obtained from the beam wings.

Acknowledgments

Authors acknowledge funding from grant Nos. III45016 and OI171038 of the Ministry of Education and Science of the Republic of Serbia and Scopes JRP IZ7370_127942.

References

[1] Fleischhauer M, Imamoğlu A and Marangos J P 2005 *Rev. Mod. Phys.* **77** 633
[2] Phillips D F, Fleischhauer A, Mair A, Walsworth R L and Lukin M D 2001 *Phys. Rev. Lett.* **86** 783
[3] Scully M O, Zhu S and Gavrielides A 1989 *Phys. Rev. Lett.* **62** 2813
[4] Harris S E, Field J E and Imamoğlu A 1990 *Phys. Rev. Lett.* **64** 1107
[5] Schmidt H and Imamoğlu A 1996 *Opt. Lett.* **21** 1936
[6] Knappe S, Shah V, Schwindt P D, Holberg L, Kitching J, Liew L A and Moreland J 2004 *Appl. Phys. Lett.* **75** 1460
[7] Fleischhauer M, Matsko A V and Scully M O 2000 *Phys. Rev.* A **62** 013808
[8] Dupont-Roc J, Haroche S and Cohen-Tannoudji C 1969 *Phys. Lett.* A **28** 638
[9] Cohen-Tannoudji C, Dupont-Roc J, Haroche S and Laloë F 1970 *Rev. Phys. Appl.* **5** 102
[10] Weis A and Karnosky S I 1992 *J. Opt. Soc. Am.* B **10** 716
[11] Budker D, Gawlik W, Kimball D F, Rochester S M, Yashchuk V V and Weis A 2002 *Rev. Mod. Phys.* **74** 1153
[12] Castagna N and Weis A 2011 *Phys. Rev.* A **84** 053421
[13] Klein M, Hohensee M, Phillips D F and Walsworth R L 2011 *Phys. Rev.* A **83** 013826
[14] Klein M J 2009 Slow and stored light in atomic vapour cells *PhD Thesis* Harvard University
[15] Gawlik W, Kowalski J, Neumann R and Trager F 1974 *Opt. Commun.* **12** 400
[16] Budker D, Yashchuk V and Zolotorev M 1998 *Phys. Rev. Lett.* **81** 5788
[17] Varzhapetyan T S, Li H, Ariunbold G O, Sautenkov V A, Rostovtsev Y V and Scully M O 2009 *Opt. Commun.* **282** 39
[18] Li H, Sautenkov V A, Varzhapetyan T S, Rostovtsev Y V and Scully M O 2008 *J. Opt. Soc. Am.* B **25** 1702
[19] Auzinsh M, Budker D and Rochester S 2010 *Optically Polarized Atoms. Understanding Light–Atom Interactions* (New York: Oxford University Press)
[20] Novikova I, Walsworth R L and Xiao Y 2012 *Laser Photon. Rev.* **6** 333
[21] Li L, Peng X, Lin C, Guo H and Chen X 2004 *J. Phys. B: At. Mol. Opt. Phys.* **37** 1873
[22] Pack M V, Camacho R M and Howell J C 2007 *Phys. Rev.* A **76** 013801
[23] Javan A, Kocharovskaya O, Lee H and Scully M O 2002 *Phys. Rev.* A **66** 013805
[24] Ye C Y and Zibrov A S 2002 *Phys. Rev.* A **65** 023806
[25] Taichenachev A V, Tumaikin A M, Yudin V I, Stahler M, Wynands R, Kitching J and Hollberg L 2004 *Phys. Rev.* A **69** 024501
[26] Radonjić M, Arsenović D, Grujić Z and Jelenković B M 2009 *Phys. Rev.* A **79** 023805
[27] Levi F, Godone A, Vanier J, Micalizio S and Modugno G 2000 *Eur. Phys. J.* D **12** 53
[28] Gilles H, Cheron B, Emile O, Bretenaker F and Floch A L 2001 *Phys. Rev. Lett.* **86** 1175
[29] Dicke R H 1748 *Phys. Rev.* **89** 472
[30] Erhard M and Helm H 2001 *Phys. Rev.* A **63** 043813
[31] Xiao Y, Novikova I, Phillips D F and Walsworth R L 2006 *Phys. Rev. Lett.* **96** 043601
[32] Xiao Y, Novikova I, Phillips D F and Walsworth R L 2008 *Opt. Express* **16** 14128
[33] Figueroa E, Vewinger F, Appel J and Lvovsky A L 2006 *Opt. Lett.* **17** 2625
[34] Vanier J, Godone A and Levi F 1998 *Phys. Rev.* A **58** 2345
[35] Novikova I, Phillips D F, Zibrov A S, Walsworth R L and Yudin V I 2006 *Opt. Lett.* **31** 2353
[36] Taichenachev A V, Yudin V I, Wynands R, Stahler M, Kitching J and Hollberg L 2003 *Phys. Rev.* A **67** 033810
[37] Failache H, Valente P, Ban G, Lorent V and Lezama A 2003 *Phys. Rev.* A **67** 043810
[38] Logg A and Wells G N 2010 *ACM Trans. Math. Softw.* **37** 20:1–20:28
[39] Logg A, Mardal K-A and Wells G N 2012 *Automated Solution of Differential Equations by the Finite Element Method (Lecture Notes in Computational Science and Engineering* vol 84*)* (Berlin: Springer)
[40] Mortensen M, Langtangen H P and Wells G N 2011 *Adv. Water Resources* **34** 1082
[41] Petelski T, Fattori M, Lamporesi G, Stuhler J and Tino G M 2003 *Eur. Phys. J.* D **22** 279
[42] Wasik G, Gawlik W, Zachorowski J and Zawadzki W 2002 *Appl. Phys.* B **75** 613
[43] Krmpot A J, Ćuk S M, Nikolić S N, Radonjić M, Slavov D G and Jelenković B M 2009 *Opt. Express* **17** 22491
[44] Matsko A B, Novikova I, Scully M O and Welch G R 2001 *Phys. Rev. Lett.* **87** 133601
[45] Matsko A B, Novikova I and Welch G R 2002 *J. Mod. Opt.* **49** 367
[46] Kazakov G, Masets I, Rozhdestvensky Yu, Mileti G, Delporte J and Matisov B 2005 *Eur. Phys. J.* D **35** 445
[47] Krmpot A J, Radonjić M, Ćuk S M, Nikolić S N, Grujić Z D and Jelenković B M 2011 *Phys. Rev.* A **84** 043844